# Stimulated slowing of Yb atoms on the narrow $^1S_0 \rightarrow {}^3P_1$ transition

Tanaporn Na Narong [1,*], TianMin Liu, Nikhil Raghuram [†], and Leo Hollberg [‡]
*Hansen Experimental Physics Laboratory, Department of Physics, Stanford University, Stanford, California 94305, USA*

(Received 21 September 2021; accepted 1 November 2021; published 29 November 2021)

We analyzed bichromatic and polychromatic stimulated forces for laser cooling and trapping of Yb atoms using only the narrow $^1S_0 \rightarrow {}^3P_1$ transition. Our model is based on numerical solutions of optical Bloch equations for two-level atoms driven by multiple time-dependent fields combined with Monte Carlo simulations, which account for realistic experimental conditions such as atomic beam divergence, geometry, and Gaussian laser modes. Using 1 W of laser power, we predict a loading rate of $\approx 10^8$ atoms/s into a 556-nm magneto-optical trap (MOT) with a slowing force of $\approx 60F_{\text{rad}}$. We show that a square-wave modulation can produce similar stimulated forces with almost twice the velocity range and improve the MOT loading rate of Yb atoms by up to 70%.

DOI: 10.1103/PhysRevA.104.053117

## I. INTRODUCTION

Cold-atom systems and quantum sensors rely upon sources of low-velocity atoms with well-controlled motional degrees of freedom. Magneto-optical traps (MOTs) are the starting point of many experiments including atomic clocks, atom interferometry, optical lattices, tweezers, fountains, and quantum degenerate gases. In this paper we analyze a promising method to reduce the complexity of cold-atom sources for Yb while maintaining good atom numbers and low temperatures. Aspects of the approach may be applicable to other atomic systems.

Many approaches have been developed to create better cold-atom sources with goals of increasing cold-atom flux, MOT loading rates, atom densities, and/or decreasing temperatures. Laser cooling is often done in two stages for closed-shell, alkaline-earth-metal-like atoms (e.g., Ca, Sr, Yb), which are of current interest for optical atomic clocks [1], quantum gases [2,3], quantum measurements [4], and atom interferometry [5,6]. The first stage cools on a broad transition to produce fast momentum transfers and large slowing forces. The second stage cools on a narrow transition to reach lower temperatures (in microkelvin for Yb and Sr). The energy level diagram for Yb in Fig. 1 shows the first-stage cooling transition $^1S_0 \rightarrow {}^1P_1$ at 399 nm and the second-stage cooling transition $^1S_0 \rightarrow {}^3P_1$ at 556 nm.

Previous laser cooling methods developed to improve loading efficiency for MOTs that trap Yb and other alkaline-earth-metal-like atoms include tailored Zeeman slowers [7–9] and preloading 2D-MOTs [10]. Other methods include adiabatic rapid passage [11–17], Sisyphus-like deceleration [18], two-photon cooling [19], two-color cooling [20,21], and quenched narrow-line cooling [22–24] that takes advantage of the narrower transitions to achieve very low temperatures. Combining several of these techniques can produce an ultracold atom source with higher phase-space densities [25]. With these approaches, experimental systems usually require multiple lasers: a first-stage cooling laser, a second-stage cooling laser, and sometimes repumping lasers to retrieve atoms from

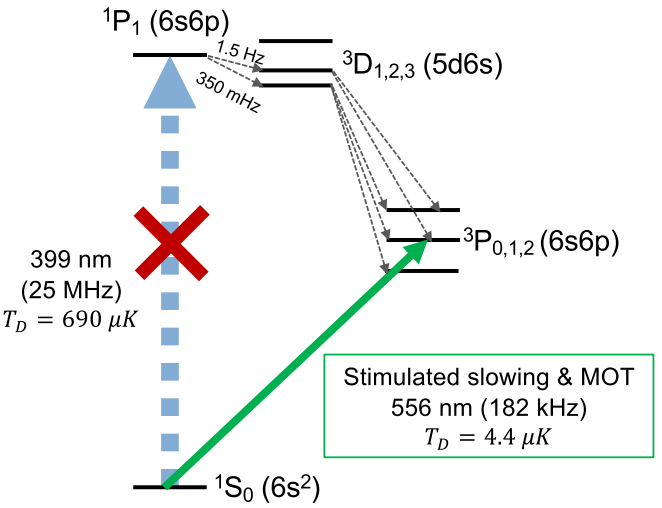


FIG. 1. Energy-level diagram of Yb showing the $^1S_0 \rightarrow {}^3P_1$ transition (green solid arrow), which is used for both stimulated slowing and magneto-optical trapping. The stimulated slowing method eliminates the need for the traditional first-stage cooling on the $^1P_1$ transition and helps avoid population loss via decays from $^1P_1$ to the lower-lying triplet $D$ states, $^3D_{2,1}$ ($5d6s$), which can lead to further decays to dark $^3P_{2,0}$ states where atoms are lost from the cooling cycles or MOTs without repumping.

*tn282@stanford.edu
†Present address: Department of Physics, Virginia Polytechnic Institute and State University, Blacksburg, VA 24061.
‡leoh@stanford.edu

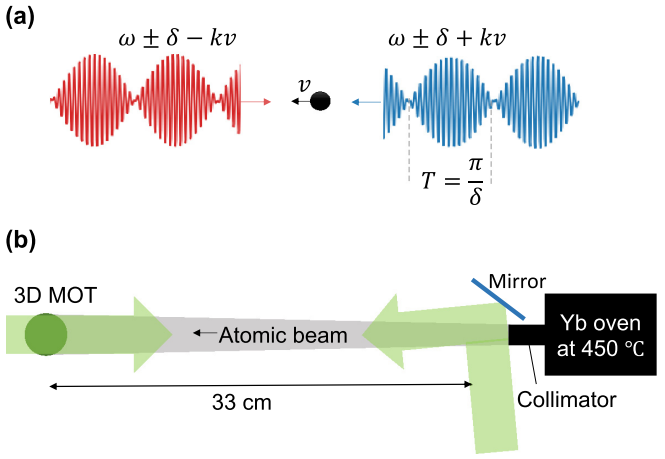


FIG. 2. (a) An atom traveling in counterpropagating bichromatic light fields with a velocity $v$. The laser beam frequencies are detuned by $+kv$ and $-kv$ to compensate for Doppler shifts. (b) A schematic diagram of our experimental setup showing a Yb atomic beam leaving an oven at 450 °C and two counterpropagating laser beams at 556 nm. The atoms are slowed over a distance of 33 cm before reaching the MOT region. Our current Yb atomic beam is partially collimated by a tubular array nozzle and diverges with a half-angle $\approx$17 mrad.

dark states. As shown in Fig. 1, Yb atoms can decay from the $^1P_1$ state to the lower-lying triplet $D$ states, $^3D_{2,1}$, and may end up in the dark $^3P_{2,0}$ states. Removing the first-stage cooling will avoid the dark-state losses and allow for a more compact system with only one cooling laser.

Our goal is to eliminate the first-stage cooling on the $^1S_0 \rightarrow {}^1P_1$ transition and only use the narrow $^1S_0 \rightarrow {}^3P_1$ transition for both slowing and trapping of Yb atoms while maintaining a high loading rate into the MOT. One limitation of laser cooling on this narrow transition is that the spontaneous optical forces are limited by the relatively small linewidth $\gamma = 2\pi \times 182$ kHz. To overcome this limit, driving stimulated transitions in atoms at much higher rates than the spontaneous decay rate can produce a slowing force $F \gg F_{\text{rad}} = \hbar k\gamma/2$. We theoretically demonstrate in this paper that using stimulated methods on the narrow $^1S_0 \rightarrow {}^3P_1$ transition in Yb can produce large forces and a high loading rate into the MOT.

Stimulated slowing methods with atomic beams [26] have been demonstrated on alkali-metal atoms [27–32] and metastable helium [33–35] but not on alkaline-earth-metal-like atoms. Recent efforts have extended the concepts [36–42] and experiments [43,44] for both atoms and molecules. Stimulated emissions can be driven by ultrashort $\pi$ pulses [45–47] or bichromatic continuous-wave (cw) beams. Following the early observations on Na [27,28], Söding *et al.* decelerated Cs atoms with a stimulated force $\approx 10F_{\text{rad}}$ using counterpropagating, bichromatic light fields with symmetric detunings $\pm\delta$ [29]. That same setup was used in the first part of our analysis, as shown in Fig. 2(a). Söding *et al.* also developed computer simulations to calculate the stimulated forces by solving the optical Bloch equations (OBEs) for two-level systems. Those simulations were adopted and applied to later bichromatic slowing experiments by Metcalf and his colleagues. They studied and measured the bichromatic force (BCF) in more detail on Rb [30,31] and He* [33,34] atoms. They also developed a theoretical model of BCF using a dressed-atom picture [48], which predicted the velocity range of the BCF more accurately than the intuitive $\pi$-pulse interpretation, which treats the bichromatic waves as individual nonoverlapping pulses. More recent experiments optimized bichromatic slowing further to enhance the Rb MOT loading rate [32] and extend the velocity range of BCF to over 300 m/s using laser frequency chirp [35]. We discuss in Sec. III A how we applied the chirped BCF method on Yb for efficient MOT loading.

We developed computer simulations of stimulated slowing of Yb atoms using only the narrow 556-nm transition for both slowing and trapping with a MOT. We first describe our model in Sec. II. Because the $^1S_0 \rightarrow {}^3P_1$ transition in Yb is nearly closed, a two-level model is well suited to describe the system. We developed Monte Carlo simulations to predict the MOT loading rate and inform the experimental design for our existing AOSense atomic beam system [Fig. 2(b)]. Section III A outlines the chirped BCF method [35] and how we optimized the MOT loading rate by choosing experimental parameters such as bichromatic detuning $\delta$, slowing beam diameters, and beam intensities, under physical constraints including the Gaussian beam profile, gravity, and limited optical power. Using 1 W of laser power, the chirped BCF method using only the 556-nm laser can achieve a loading rate of $10^8$ atoms/s, which is comparable to the loading rate into a 556-nm MOT achieved by a 399-nm Zeeman slower [49]. We analyze other approaches to improve the stimulated forces and the MOT loading rate in the later sections.

Our analysis extends beyond the bichromatic force to polychromatic forces in Sec. III B. Inspired by the four-color stimulated forces presented in [37], we demonstrate that adding higher odd harmonics of the bichromatic light via a square-wave amplitude modulation roughly doubles the velocity range of the force and improves the MOT loading rate by 70% compared to the chirped BCF method with the same total laser power. We also discuss the time evolution of the two-level atom in the square-wave amplitude-modulated light fields using Bloch vector trajectories. We show in Sec. III C that a square-wave phase modulation produced similar stimulated forces, which opens up a possibility of utilizing phase modulators in stimulated slowing experiments. To broaden the velocity range of the force, we explored a broadband cooling approach that superposes two BCF profiles at two different detunings. Although our calculations show that interference makes BCF vanish for a single two-level system [34], broadband cooling may be feasible in molecules and more complex multilevel systems [42]. Overall, our simulation results provide insights into bichromatic and square-wave stimulated forces on two-level atoms and inform the experimental design that optimizes the loading rate of Yb atoms into the MOT using only the 556-nm laser.

## II. NUMERICAL MODEL

To investigate different stimulated slowing approaches, we developed our initial model in Python to calculate the BCF on two-level atoms. Similar to what was implemented in [29],

our initial model assumes a two-level atom traveling in a bichromatic standing wave. Each amplitude-modulated wave consists of two beating frequencies $\omega \pm \delta$, which are detuned to compensate for the Doppler shifts [Fig. 2(a)]. Other key parameters include the Rabi frequency $\Omega$ and relative phase $\chi$ between the blue-detuned and red-detuned light fields.

The force on an atom is calculated numerically from the density matrix, $\rho(t)$, and the two-level atom's Hamiltonian, $H(t)$. We applied the rotating wave and dipole approximations on the $2 \times 2$ Hamiltonian matrix. When the bichromatic light fields are detuned by $\pm\delta$ from resonance, the diagonal terms $H_{00}$ and $H_{11}$ of $H(t)$ are zero. The off-diagonal components $H_{01} = H_{10}^{\dagger}$ are given by

$$H_{01} = \frac{\Omega}{2}[e^{-ikz}(e^{i(\delta t+\chi)} + e^{-i(\delta t+\chi)}) + e^{ikz}(e^{i\delta t} + e^{-i\delta t})]$$
$$= \Omega[e^{-ikz}\cos(\delta t + \chi) + e^{ikz}\cos(\delta t)], \quad (1)$$

where the Rabi frequency $\Omega = \frac{eE_0}{\hbar}\langle 1|r|0\rangle$ and $E_0$ is the electric field amplitude of each of the four cw beams. We assume the electric field amplitude $E_0$, hence Rabi frequency $\Omega$, of each of the slowing beams to be identical. The effects of power imbalance on stimulated forces were discussed in [37], where they found that the stimulated forces decreased when the beams were imbalanced.

We then solve the OBEs for the density matrix $\rho$ using a built-in Linblad master equation solver from the QuTip library [50,51]. The Linblad master equation is given by

$$\dot{\rho}(t) = -i\hbar[H(t), \rho(t)] + \tfrac{1}{2}[2C\rho(t)C^{\dagger} - \rho(t)C^{\dagger}C - C^{\dagger}C\rho(t)]. \quad (2)$$

In Eq. (2), spontaneous emissions are included via a collapse operator $C = \sqrt{\gamma}|0\rangle\langle 1|$, where $|0\rangle$ and $|1\rangle$ denote a two-level atom's ground and excited states, respectively. After solving Eq. (2) for $\rho$, the force is computed from $F(t) = \hbar\frac{\partial}{\partial z}\mathrm{Tr}(\rho H)$. We found that setting $\Omega/\delta = \sqrt{3/2}$ and $\chi = \pi/4$ optimized the magnitude and velocity range of the BCF. Our results are consistent with previous numerical work [29,37,48]. Figure 3 shows the stimulated forces plotted against atomic velocity for three different values of $\delta$ and the respective Rabi frequency $\Omega = \sqrt{3/2}\delta$. At this optimal ratio and phase $\chi = \pi/4$, the magnitude of the bichromatic force is given by

$$F_{\mathrm{BCF}} = \frac{\hbar k\delta}{\pi}. \quad (3)$$

Since we can choose $\delta \gg \gamma$, $F_{\mathrm{BCF}}$ can be much larger than the radiative force $F_{\mathrm{rad}} = \hbar k\gamma/2$ and have a broad velocity range of $\Delta v \sim \delta/2k \gg \gamma/k$ [48]. The red (upper) curve in Fig. 3 corresponds to $\delta = 150\gamma$ and $\Omega = 184\gamma \approx 2\pi \times 33$ MHz, which produces a BCF with magnitude $\approx 90F_{\mathrm{rad}}$. Another key feature of the BCF is sharp Doppleron resonances at velocities $v = \pm\delta/(2n+1)k$, $n = 0, 1, 2, \ldots$ [52]. Nevertheless, these sudden increases in the stimulated force were not observed in bichromatic force measurements [30,31] and do not affect the slowing process significantly.

Both the magnitude and velocity range of the bichromatic force show promise for stimulated slowing in loading atoms into a MOT [32]. We estimate the MOT loading efficiency for Yb atoms using Monte Carlo simulations with roughly

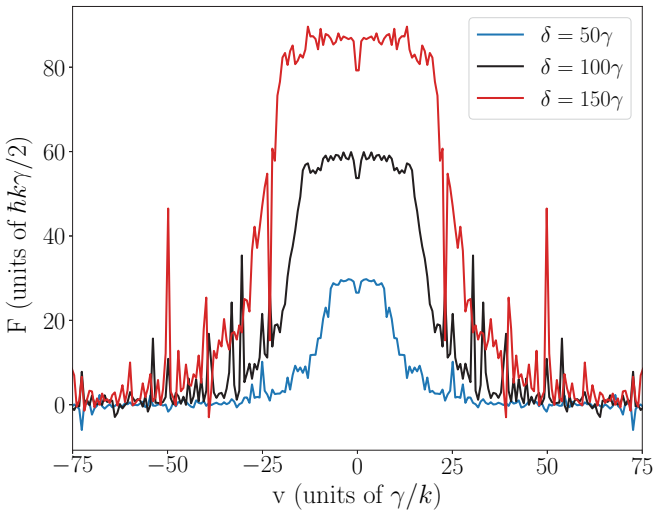


FIG. 3. Bichromatic force as a function of atomic velocity for $\delta = 50\gamma$ (blue, lower line), $100\gamma$ (black, middle line), $150\gamma$ (red, upper line), Rabi frequency $\Omega = \sqrt{3/2}\delta$, $\chi = \pi/4$. The magnitude and range of the force scale linearly with $\delta$. At $\delta = 150\gamma$ and $\Omega = 184\gamma$ (red, upper line), the maximum stimulated force is near $90F_{\mathrm{rad}}$ and acts over the velocity range of $\pm 30\gamma/k \approx 3$ m/s for the $^1S_0 \rightarrow {}^3P_1$ transition in Yb.

20 000 atoms. For an individual atom with a given velocity and position, we compute the bichromatic force by following the above procedure and then integrate the force to update the atom's velocity and position at every 10-$\mu$s interval. This time interval is approximately the time it takes for an atom's velocity to change by $\gamma/k$ under the stimulated force.

Our simulations account for realistic experimental conditions as illustrated in Fig. 2(b). Yb atoms leave a 450 °C oven, where the total atomic beam flux from the collimator is $10^{11}$ atoms/s, and travel in a bichromatic light field, defined by the key parameters $\delta$ and Rabi frequency $\Omega$, towards a three-dimensional (3D) 556-nm MOT located 33 cm away from the oven aperture that has a small diameter of 4 mm. The atomic beam is slowly diverging with 17 mrad half-angle divergence. We take into account the laser's Gaussian beam profile, which causes a spatial variation in laser intensity and hence Rabi frequency $\Omega$. We assume in this analysis that the spectral linewidth of the laser is much smaller than the natural linewidth $\gamma$ of the $^1S_0 \rightarrow {}^3P_1$ transition, which is 182 kHz. Our model includes the effects of gravity. Monte Carlo simulations enabled us to estimate the fraction of atoms that are slowed to the MOT's capture velocity and the respective loading rate. To estimate the MOT's capture velocity, we use the 556-nm MOT parameters from [49]: the MOT detuning of $-4.6$ MHz and axial magnetic field gradient of 3.4 G/cm. Assuming a MOT beam diameter of 2 cm, to achieve the beam intensity of $I = 100I_{\mathrm{sat}}$ ($I_{\mathrm{sat}} = 0.136$ mW/cm$^2$ for this transition) in each of the three MOT beams requires a total optical power of 130 mW. With these parameters, we estimate the MOT's capture velocity to be $\approx 5$ m/s.

We have estimated the effects of momentum diffusion due to spontaneous emission. Due to the relatively long lifetime of the $^3P_1$ state (874 ns), Monte Carlo simulations estimate that an atom in resonance with the bichromatic light fields

undergoes up to 49 000 stimulated and 1600 spontaneous emissions in the slowing duration of 3 ms. With the recoil velocity of 4 mm/s/photon, we estimate the random diffusion velocity to be ≈16 cm/s, which is negligible for this system. These effects are even smaller when atoms are driven by square-wave amplitude-modulated light (Sec. III B). In that case, the number of spontaneous emissions is reduced by 33% and the estimated random diffusion velocity decreases to 13 cm/s. The heating effects from momentum diffusion would be more prominent for atoms with shorter lifetimes. For Yb, we neglected these effects and focused our efforts on achieving a large velocity slowing range (e.g., 200 m/s) and optimizing the loading rate into the MOT. We discuss several approaches as follows.

## III. RESULTS AND DISCUSSION

### A. Chirped BCF

Chieda and Eyler demonstrated on He* atoms that laser frequency chirp can extend the velocity range of stimulated slowing without requiring a very large bichromatic detuning $\delta$ [35]. The laser frequency was swept in a sawtooth manner to keep the laser detuning in resonance with the moving atoms while they are being slowed. This method can extend the slowing velocity range from a few 10 m/s to $>$ 200 m/s without requiring larger $\delta$ and Rabi frequency $\Omega$. Although the time dependence of the chirp method does not capture all of the atoms, the method does reduce the power requirement and avoids the large $\delta$ regime where the bichromatic force reportedly vanishes [35].

Our Monte Carlo simulation results in Fig. 4 show that laser frequency chirp can significantly increase the slowing range and fraction of slow atoms below the MOT capture velocity 5 m/s. In our simulations, the laser frequency chirp follows a sawtooth function with a period of a few milliseconds with 100% duty cycle. In Fig. 4(a), the laser detuning was fixed at 240 m/s. Even at $\delta = 200\gamma$ and $\Omega = 244\gamma$, the affected atoms were only slowed by a few 10 m/s range, and not surprisingly the number of atoms near zero velocity remained unchanged. In contrast, sweeping the detuning from 240 to 10 m/s in 2 ms substantially broadened the slowing velocity range and increased the population of atoms with velocities below the capture velocity of 5 m/s by at least four orders of magnitude. This result demonstrates that the laser frequency chirp method is an effective method in loading the MOT. Our simulations also enabled us to investigate how other experimental conditions, such as the laser beam profile, affect the MOT loading rate.

As Figs. 4(b) and 4(c) show, with stimulated slowing the realistic laser Gaussian beam profile reduces the MOT loading rate relative to an unrealistic uniform intensity profile. Because the stimulated force is strongly dependent on the $\Omega/\delta$ ratio and the Rabi frequency $\Omega$ rapidly decays with the atoms distance from the beam axis, only atoms near the center of the beam experience a significant force and are slowed to the target capture velocity. In this particular example, the MOT loading rate was roughly five times smaller when using the Gaussian beam profile [Fig. 4(b)] compared to the flattop beam profile [Fig. 4(c)], in which Rabi frequency $\Omega$ remains

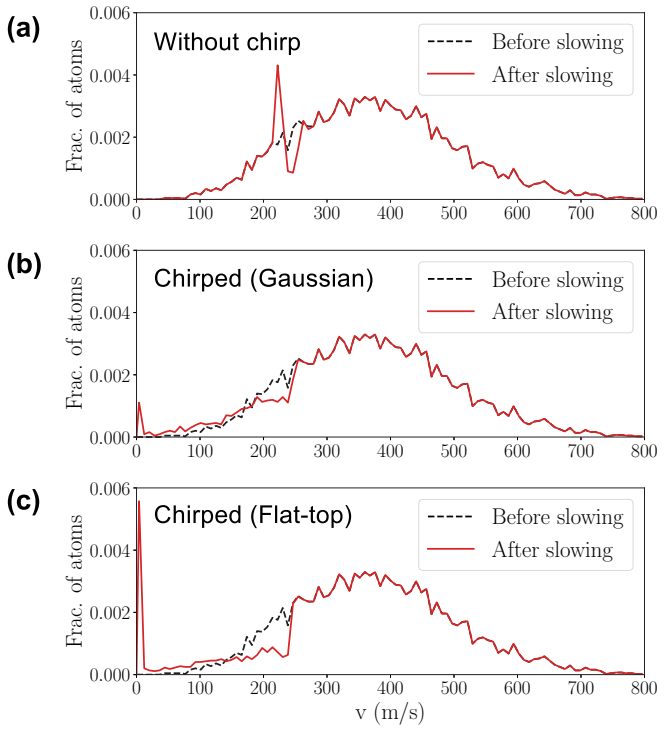


FIG. 4. Velocity distributions before (black dashed line) and after (red solid line) slowing with (a) a fixed detuning at 240 m/s and (b) chirped detuning from 240 to 10 m/s in 2 ms. Gaussian beam diameter of 8 mm, $\delta = 200\gamma$, and peak Rabi frequency $\Omega = 244\gamma$ for both (a) and (b). (c) Same chirp parameters and laser power as (b) but with a flattop beam profile of the same diameter. Rabi frequency $\Omega = 173\gamma$ is constant across the beam profile and $\delta$ was adjusted to $141\gamma$. The unrealistic assumption of a flattop beam profile overestimated the MOT loading rate. It is important to take into account the actual Gaussian beam profile.

constant and optimized across the beam area. Both simulations used the same chirped detuning from 240 to 10 m/s, the same laser power, and the same beam diameter of 8 mm, which was twice as large as the oven aperture diameter of 4 mm, to compensate for the atomic beam divergence and maximize the number of atoms slowed. In addition to the laser power, geometric constraints of the experimental hardware must be taken into account to optimize the loading rate into the MOT.

To optimize the slowing force on atoms and the MOT loading rate, we kept the $\delta/\Omega$ ratio at $\sqrt{3/2}$ at the center of the Gaussian beam. The Rabi frequency $\Omega$ is proportional to the square root of the laser intensity. Therefore, $\delta$, $\Omega$, and hence the stimulated force, are limited by laser intensity. For a fixed laser power, there is a trade-off between laser intensity, which sets the magnitude of the slowing force, and laser beam size, which determines the area across the laser beam profile where the force is present. Chirp parameters including the chirped detuning range and chirp period also play a role. A high laser intensity and large force allow a higher chirp rate, which means the starting detuning can be set to a higher velocity to slow a larger fraction of atoms that follow the effusion velocity distribution $f(v) \propto v^3 \exp(-mv^2/k_BT)$. Therefore, the fraction of atoms in the atomic beam that will be slowed is

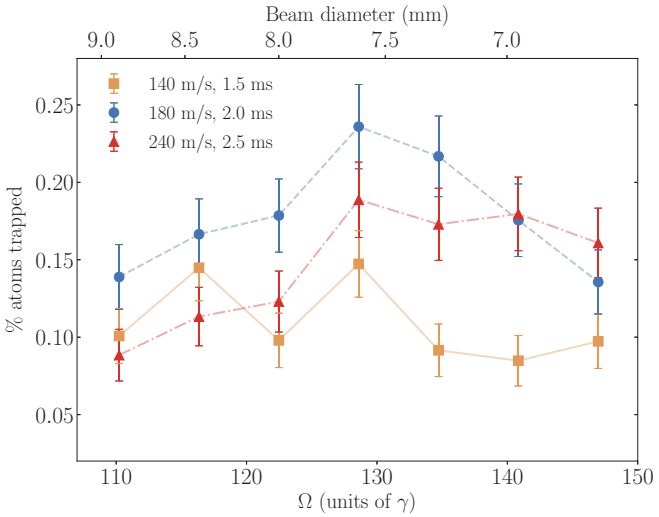


FIG. 5. Percentage of atoms in the atomic beam that can be trapped by the 556-nm MOT after bichromatic slowing plotted against Rabi frequency Ω and laser beam diameter for three different chirp settings: 140 → 10 m/s in 1.5 ms (square, solid line), 180 → 10 m/s in 2 ms (circle, dashed line), and 240 → 10 m/s in 2.5 ms (triangle, dot-dashed line). The error bars represent 95% confidence interval. Using 1 W of laser power, up to 0.24% of atoms can be trapped using $\delta = 105\gamma$, $\Omega = 129\gamma$ with a Gaussian beam $1/e$ diameter of 7.6 mm and a laser detuning chirp from 180 to 10 m/s in 2 ms.

strongly dependent on the choice of chirp parameters as well as $\delta$, $\Omega$, and the laser Gaussian beam diameter.

Under realistic experimental constraints including the Gaussian beam profile and total laser power of 1 W distributed equally between the stimulated slowing beams, we determined $\delta$, $\Omega$, and chirp parameters that optimized the loading rate of atoms into a 556-nm MOT. Figure 5 shows some of the best results predicted by our Monte Carlo simulations of more than 20 000 atoms, using three different chirp settings: 140 → 10 m/s in 1.5 ms (square, solid line), 180 → 10 m/s in 2 ms (circle, dashed line), and 240 → 10 m/s in 2.5 ms (triangle, dot-dashed line). The error bars shown on the plot represent the 95% binomial confidence interval. We found that the optimal settings for bichromatic slowing of Yb for the optical power limit of 1 W were $\delta = 105\gamma$, $\Omega = 129\gamma$ with a Gaussian beam $1/e$ diameter of 7.6 mm, and a laser detuning chirp from 180 to 10 m/s in 2 ms. With these settings, up to $0.24 \pm 0.03\%$ of the total atomic flux from the oven can be trapped by the 556-nm MOT with the capture velocity of 5 m/s.

Assuming an atomic flux of $10^{11}$ atoms/s leaving the oven (as observed experimentally), the predicted loading rate of 0.24% is equivalent to $2.4 \times 10^8$ atoms/s. This MOT loading rate using the chirped bichromatic slowing method is comparable to the 556-nm MOT loading rate achieved using a conventional 399-nm Zeeman slower [49]. We were encouraged by the results by Kawasaki *et al.* who showed that loading Yb directly into a 556-nm MOT without first-stage cooling was possible, but the loading rates were low (under $10^4$ atoms per second) [53]. Our simulation results so far have shown that bichromatic slowing with the 556-nm laser may be able to replace a 399-nm Zeeman slower in loading Yb atoms into the MOT. We also explore different approaches to improve this stimulated slowing method. We show in Sec. III B that a square-wave amplitude modulation can produce a polychromatic stimulated force that improves the MOT loading rate even further.

### B. Square-wave amplitude modulation

Although the bichromatic force is already an effective method for stimulated slowing of Yb atoms, this force can be enhanced by adding higher harmonics of the bichromatic light [37]. Galica *et al.* presented numerical calculations of a four-color polychromatic force [37], which has a larger magnitude and broader velocity range than BCF, and is produced by adding the third harmonic of the bichromatic detuning $\delta$ to make the pulses narrower in time and more similar to separate $\pi$ pulses. Their results motivated us to investigate the use of square-wave modulation and the effects of adding higher harmonics on stimulated forces on Yb.

Starting from the BCF model we developed, we modified the Hamiltonian to describe square amplitude-modulated light. The cosine amplitude modulation terms in Eq. (1) are replaced by a square-wave modulation at frequency $\delta_{\rm sq}$. The light fields now consist of two counterpropagating beams, each with Rabi frequency $\Omega$, a square amplitude modulation at frequency $\delta_{\rm sq}$, and a phase difference $\chi$ between each beam. We investigated both near-ideal square waves produced by a built-in square-wave function in the SciPy signal processing library and approximations from a truncated Fourier series of a square wave. The Fourier series that contains $n$ harmonics consists of odd harmonics $\pm\delta_{\rm sq}, \pm 3\delta_{\rm sq}, \pm 5\delta_{\rm sq}, \ldots, \pm(2n-1)\delta_{sq}$ with decreasing amplitudes. For example, a square wave with only two harmonics ($n = 2$) has frequency components $\pm\delta_{\rm sq}$ and $\pm 3\delta_{\rm sq}$ with Rabi frequencies $\Omega$ and $\Omega/3$, respectively. One limitation of the square-wave modulation is that we cannot specify the amplitudes or phases of different harmonics independently. We show later that this is not a problem provided we find the right $\Omega$ and $\chi$. The off-diagonal element $H_{01}^{\rm sq}$ of the new Hamiltonian now contains the square-wave Fourier series, and is given by

$$H_{01}^{\rm sq}(z,t) = \Omega e^{-ikz} \sum_{i=1}^{n} \frac{4}{\pi(2i-1)} \sin\left((2i-1)(\delta_{\rm sq}+\chi)\right) + \Omega e^{ikz} \sum_{j=1}^{n} \frac{4}{\pi(2j-1)} \sin\left((2j-1)\delta_{\rm sq}\right). \quad (4)$$

Calculating and plotting stimulated forces as a function of velocity over a parameter space spanning a Rabi frequency range $0 \leqslant \Omega \leqslant 3\delta_{\rm sq}$ and a phase range $0 \leqslant \chi \leqslant \pi$ revealed that $\Omega = \pi\delta_{\rm sq}/4 \approx 0.8\delta_{\rm sq}$ and relative phase $\chi = 0.36\pi \approx \pi/3$ optimized the magnitude and velocity range of the stimulated force. At the optimal Rabi frequency value $\Omega = \pi\delta_{\rm sq}/4$, the force-velocity profile is sensitive to the choice of phase $\chi$. Figure 6 shows the contour plot of this square-wave force as a function of the atoms velocity $v$, and phase $\chi$ in the units of $\pi$ between 0 and $\pi/2$ for $\Omega = 61\gamma$. With larger force shown in red, the plot indicates a region between $0.3\pi \leqslant \chi \leqslant 0.4\pi$ where a strong stimulated force is uniformly present over a

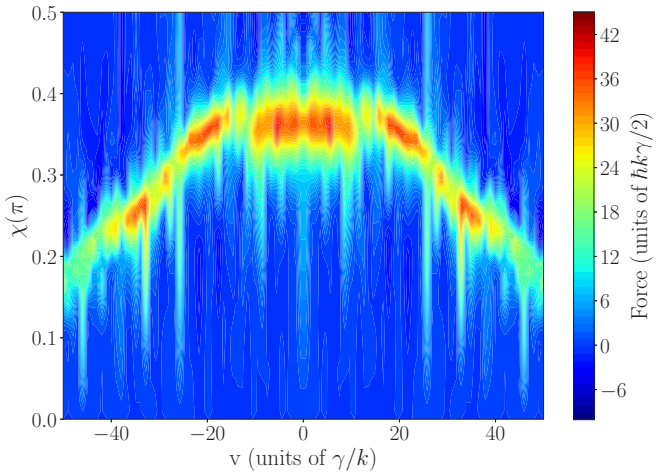


FIG. 6. Stimulated force from an approximate square-wave modulation with only the first three harmonics ($n = 3$) of $\delta_{sq}$ plotted in the parameter plane of the atoms velocity $v$ and phase $\chi$. $\Omega = \pi\delta_{sq}/4 = 61\gamma$, $\chi = 0.36\pi$ produce the strongest stimulated force with a magnitude of over $35F_{rad}$, which acts over a broad velocity range of over $\pm 25\gamma/k$.

broad velocity range of $\pm 25\gamma/k$. This width is almost twice the width at the peak of the optimal BCF force-velocity profile in Fig. 3 for $\delta = 50\gamma$ and the same Rabi frequency $\Omega = 61\gamma$ (blue, lower line). For smaller values of $\chi$, the velocity range of the square-wave force splits into two narrow domains, and the force vanishes close to $\chi = 0$ and $\pi/2$. We verified from this plot that $\chi = 0.36\pi$ optimized the force magnitude and velocity range. This optimal phase remains the same regardless of the number of harmonics $n$ present in the square wave, so we only display the $n = 3$ case in Fig. 6. The optimal $\Omega/\delta_{sq}$ ratio we found matches the $\pi$-pulse condition $\Omega = \pi\delta_{sq}/4$ described in [29,31]. When this condition is fulfilled, the arrival of each pulse inverts the atomic population between the atoms ground and excited states. Counterpropagating pulse trains keep the atom cycling between the two states as it absorbs photons from one pulse train and reemits them into the other. We confirmed this finding at the optimal conditions $\Omega = \pi\delta_{sq}/4$, $\chi = 0.36\pi$ by plotting the Bloch vector of the two-level system as a function of time. The Rabi cylinder plots in Fig. 7(a) show the time evolution of two components of the Bloch vector

$$v(t) = i(\rho_{01} - \rho_{10}),$$
$$w(t) = \rho_{11} - \rho_{00}$$

without decay for the optimum BCF, and truncated square-wave cases with only two and three harmonics $n$ in the square-wave Fourier series. The Bloch vector trajectory in the BCF case (left) shows symmetric wrapping around $w(t) = 0$ (note that our result is $\pi/2$ phase shifted relative to Galica *et al.*'s result in [37]). Starting in the ground state, the Bloch vector rotates counterclockwise and approaches the excited state, at which it reverses direction, then returns to the ground state before rapidly completing a full clockwise rotation. The plot of excited-state population $\rho_{11}$ as a function of time directly below the Bloch cylinder shows that the additional wrapping slows down the cycling between the ground and excited state. These results draw a clear distinction between the bichromatic light fields and alternating $\pi$ pulses, which would produce a simple rotation of the Bloch vector without any wrapping.

On the other hand, the Bloch vector trajectories under the optimal square-wave conditions are similar to the $\pi$-pulse-like periodic cycling between the ground and the excited state with minimal wrapping around the ground state. Figure 7(b) shows that on average, an atom spends less time in the excited state when driven by the optimal square-wave light fields. This reduces the number of spontaneous decays by 33% compared to the BCF method, and hence decreases the heating effects

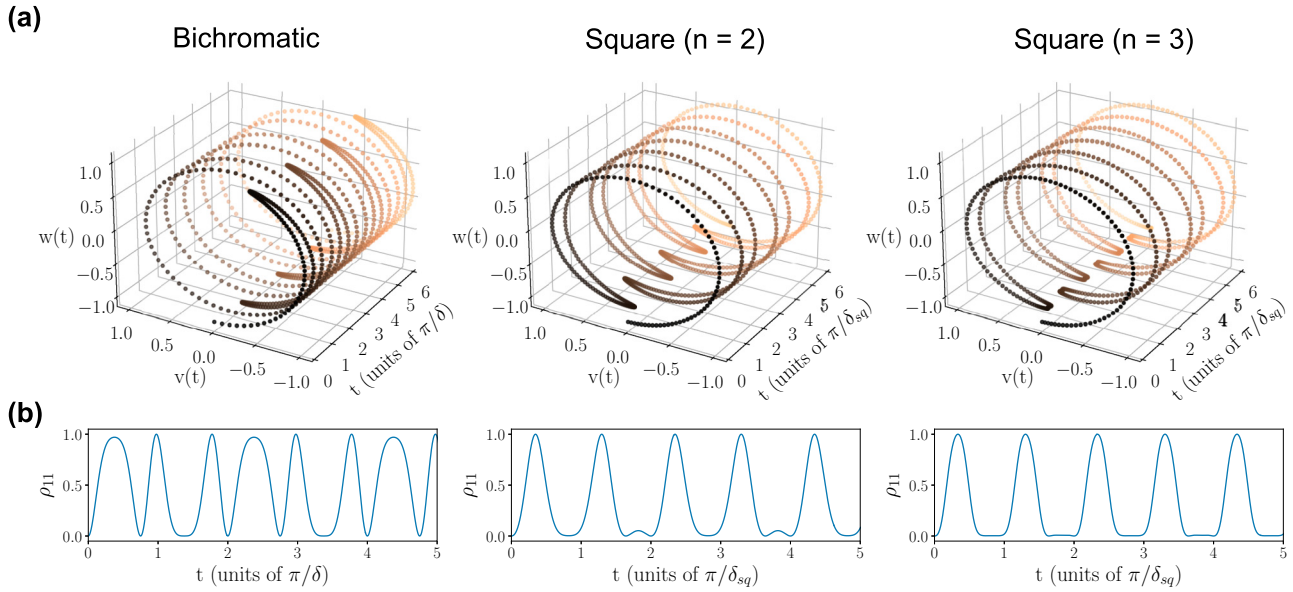


FIG. 7. Time evolution of the Bloch vector (top row) and the excited-state population $\rho_{11}$ (bottom row) for a two-level system in the optimal bichromatic (left) and square-wave light fields with the first two harmonics (center), and three harmonics (right). The spacing between dots corresponds to the time interval of 0.4 ns.

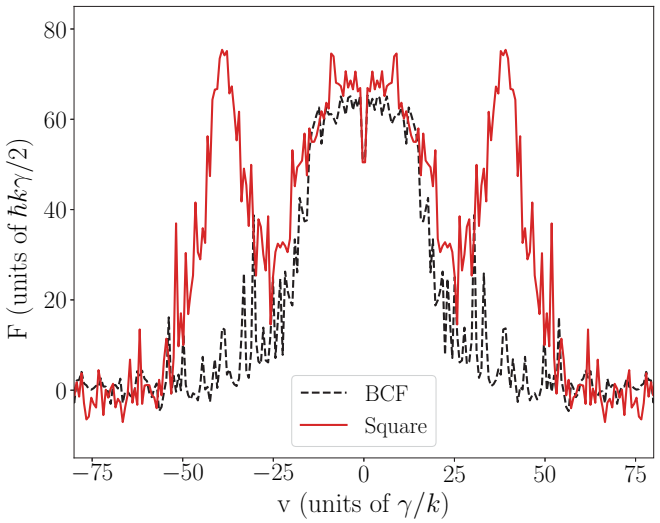


FIG. 8. Force-velocity plots showing BCF (black dashed line) and the stimulated force from a near-ideal square wave (red solid line). $\Omega = 122\gamma$ for both cases. $\delta = 100\gamma$ in the BCF case to keep $\Omega/\delta = \sqrt{3/2}$ and $\chi = \pi/4$. For the square-wave case, $\delta_{sq} = 155\gamma$ and $\chi = 0.36\pi$ to optimize the force profile.

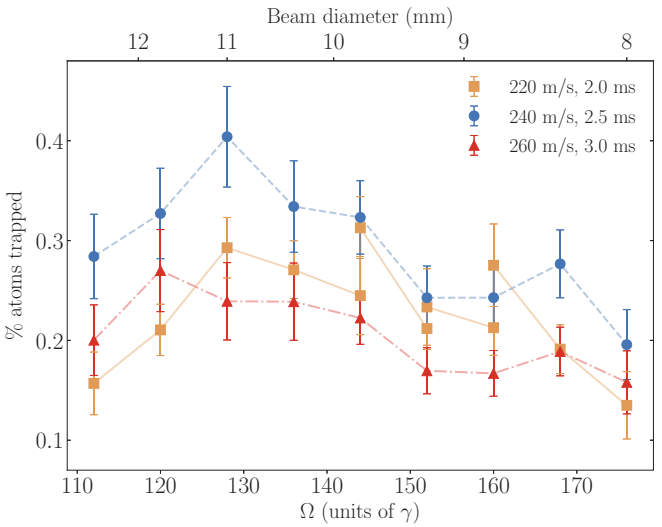


FIG. 9. Percentage of atoms in the atomic beam that can be trapped by the 556-nm MOT after slowing with the square-wave stimulated force plotted against Rabi frequency $\Omega$ and laser beam diameter for three different chirp settings: 220 → 10 m/s in 2 ms (square, solid line), 240 → 10 m/s in 2.5 ms (circle, dashed line), 260 → 10 m/s in 3 ms (triangle, dot-dashed line). Using 1 W of laser power, up to 0.40% of atoms can be trapped using $\delta_{sq} = 160\gamma$, $\Omega = 128\gamma$ with a Gaussian beam $1/e$ diameter of 11 mm, total laser power of 1 W, a slowing distance of 33 cm, and a laser detuning chirp from 240 to 10 m/s in 2.5 ms.

from momentum diffusion. The center plot in Fig. 7(a) with only two harmonics ($n = 2$) is very similar to the four-color case presented in [37], which also contains only the first and third harmonics of the bichromatic light fields. As Fig. 7(a) shows, adding the fifth harmonic ($n = 3$) suppressed the wrapping around the ground state almost entirely. The excited-state population plot below for $n = 3$ shows a simple oscillation between the ground and excited states, which is more similar to the $\pi$-pulse behavior. When even higher harmonics are present, the Bloch vector simply reverses the direction at the ground state after each complete rotation with virtually no wrapping at the ground state. Although the Bloch vector trajectories slightly differ for different number of harmonics $n$, we found that the force-velocity profile of the square-wave force, shown as the red solid curve in Fig. 8, remained the same for all $n > 2$ for $\Omega = \pi\delta_{sq}/4$ and $\chi = 0.36\pi$. Note that both the strong force and the population inversion disappear if we remove the third and all higher harmonics and revert to a sinusoidal modulation ($n = 1$) under the same conditions.

Figure 8 shows that the square-wave modulation enhances the velocity range of the stimulated force. The square-wave force (red solid curve), generated using the near-ideal square wave, has a comparable maximum magnitude comparable to the BCF of the same optical power (black dashed curve), and consists of three prominent broad peaks instead of one. The two side peaks are symmetrical around zero velocity with about half the width of the central peak, such that the total width is roughly twice that of the BCF profile. As previously stated, the square-wave force profile did not change significantly with the number of harmonics $n$ present. The $n = 2$ force profile overlapped almost perfectly with the force profile shown in Fig. 8, which was generated by the sharp-edge square-wave function from the SciPy library.

After characterizing and optimizing the square-wave force profile, we ran Monte Carlo simulations to predict and optimize the MOT loading rate. We apply the laser frequency chirp method, as described earlier in Sec. III A, to maximize the slowing velocity range. The velocity detunings $\pm kv$ in each of the two counterpropagating beams are swept in a sawtooth manner every few milliseconds to stay in resonance with atoms as they are being slowed from over 200 m/s to 10 m/s. Note that the laser frequency chirp is applied separately from the square-wave amplitude modulation. The modulation frequency $\delta_{sq}$ remains constant to satisfy the condition $\Omega = \pi\delta_{sq}/4$ while the velocity detunings change over time. Using the total optical power of 1 W and optimal Rabi frequency, laser frequency chirp velocity range, chirp rate, and Gaussian beam size, we found that up to $0.40 \pm 0.05\%$ of Yb atoms in the atomic beam can be trapped by the 556-nm MOT after being slowed by the square-wave stimulated force. Figure 9 shows the predicted loading rate as a function of Rabi frequency $\Omega$ and beam diameter for three different chirp settings: 220 → 10 m/s in 2 ms (square, solid line), 240 → 10 m/s in 2.5 ms (circle, dashed line), 260 → 10 m/s in 3 ms (triangle, dot-dashed line). The optimal conditions favor a larger $1/e$ Gaussian laser beam diameter of 11 mm compared with the BCF preferred beam diameter of 7.6 mm. Given that our atomic beam has a diameter of only 4 mm, this result highlights the pronounced effects of the Rabi frequency variation in the Gaussian beam on the stimulated force produced by a square-wave modulation.

Compared to the chirped BCF method that can produce the MOT loading rate of $2.4 \times 10^8$ atoms/s, our simulation predicts that the square-wave method can enhance the loading rate by 70% ($4.0 \times 10^8$ atoms/s) using the same laser

power and a larger Gaussian beam diameter. For the square-wave method, we have assumed that electro-optic modulators can produce the square-wave amplitude modulation on the two counterpropagating beams at the desired modulation frequency around $\delta_{sq} = 160\gamma \approx 2\pi \times 29$ MHz without losing any optical power, as opposed to splitting the laser beam into multiple laser beams and overlapping the different harmonics. This assumption allowed us to use larger beam sizes in the square-wave case, in which 1 W of laser power was split evenly between two beams instead of four beams in the BCF case. We have shown that both the square-wave and BCF methods can produce a loading rate on the order of $10^8$ atoms/s using only one 556-nm laser. The MOT loading rate might be improved further if one modifies the laser beam profile from Gaussian to flattop over the slowing distance between the oven aperture and the MOT. This is difficult in our experiment due to the long slowing distance of 33 cm.

### C. Phase modulation

Both the bichromatic and polychromatic stimulated slowing methods presented so far utilize counterpropagating amplitude-modulated light to induce stimulated emissions in atoms. In this section, we investigate a different approach using phase-modulated light.

Motivated by the promising results from Sec. III B, we first looked at a square-wave phase modulation (square-wave PM). The setup consists of two counterpropagating cw beams. The optical phase of each of the two electric fields is a square-wave oscillating between 0 and $\pi$ at a phase modulation frequency $\delta_\phi$. The relative phase $\chi$, which has a fixed value, sets the offset between the phase switching in the red- and blue-detuned fields. In the time domain, switching the optical phase between 0 and $\pi$ (square-wave PM) produces an equivalent output as a square-wave AM that alternates the sign of the amplitude between 1 and $-1$. We verified with our model that a square-wave PM can produce an identical stimulated force-velocity profile (blue solid curve in Fig. 10) to the square-wave AM force profile shown in Fig. 8, given that the phase modulation frequency $\delta_\phi$ and Rabi frequency $\Omega$ satisfy $\Omega = \pi\delta_\phi/4$ and the relative phase between the two counterpropagating beams is fixed at $\chi = 0.36\pi$. This result suggests that it is possible to replace amplitude modulators by phase modulators in a stimulated slowing experiment to produce the same force by a square-wave modulation. As with the square-wave AM, replacing the near-ideal square-wave function with a truncated Fourier series did not alter the force-velocity profile shown in Fig. 10.

We then tried replacing the square-wave modulation with a sinusoidal phase modulation (sine PM) while keeping $\pi\delta_\phi/4$ and $\chi = 0.36\pi$. As shown in Fig. 10, the force (black dashed curve) almost vanishes and no longer looks symmetrical about zero velocity. In the time domain, beside the larger wrapping of the Bloch vector near the ground state, we did not identify any striking features that could explain this asymmetry in the force-velocity profile. We have also tried searching the parameter space of $\Omega/\delta_\phi$ and $\chi$ to identify new optimizing conditions for the sinusoidal PM setting, but we have not found any conditions that the sinusoidal phase modulation can improve the stimulated force beyond the bichromatic force, or the square-wave force.

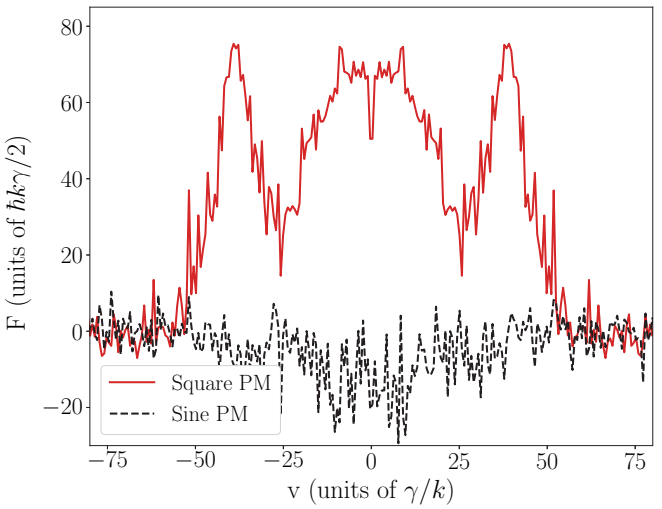


FIG. 10. Force-velocity plots for square-wave phase modulation function (red solid line) and sinusoidal phase modulation function (black dashed line). $\delta_\phi = 153\gamma$, $\Omega = 122\gamma$, and $\chi = 0.36\pi$ in both cases.

### D. Broadband cooling

To broaden the velocity range of the BCF and enhance the MOT loading rate, we also investigated a broadband cooling approach by adding bichromatic light fields at different velocity detunings. This is similar to ideas of broadband cooling that have proven useful in some cases of Doppler cooling [54–58]. However, for our configuration of stimulated slowing on a two-level atom, interference can make the force vanish if the two velocity detunings are less than $\sim 2\delta/k$ apart.

Some stimulated forces can be retrieved when the velocity detunings are further apart. Figure 11 shows the bichromatic force-velocity plots at zero-velocity detuning $v_c = 0$ (blue

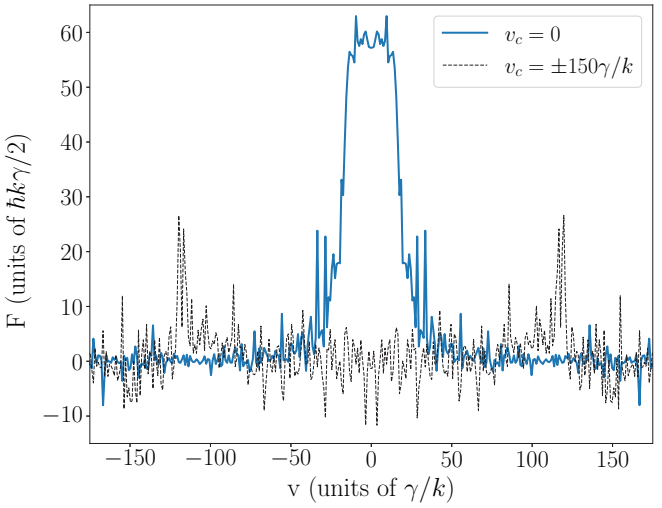


FIG. 11. Bichromatic force-velocity plots centered at zero detuning $v_c = 0$ (blue solid line) and two velocity detunings at $v_c = \pm 1.5\delta/k = \pm 150\gamma/k$ (black dashed line).

solid line) and at two velocity detunings $v_c = \pm 3\delta/2k = \pm 150\gamma/k$ (black dashed line), in this case where $\delta = 100\gamma$. We observe here that two bichromatic light fields of the same $\delta = 100\gamma$ at two detunings separated by $3\delta/k$ produce two small peaks that are much smaller and narrower than the original force profile. The minimum spacing required $\approx 2\delta/k$ to retrieve the forces is greater than the width of an individual BCF profile $\Delta v \sim \delta/2k$. Therefore, we cannot produce a broadened stimulated force on a single two-level system by simply adding more detunings at the same phase $\chi = \pi/4$.

We also verified that it was not possible to produce optical molasses on a single two-level system by combining two shifted bichromatic force profiles at the opposite phases $\chi = \pm\pi/4$. This is consistent with the findings by Partlow *et al.* [34] from their attempt to create the optical molasses force on He* atoms. To avoid interference, they had to apply the two force profiles on the atoms at two separate locations. On the other hand, as demonstrated by Wenz *et al.*, in more complicated systems such as diatomic and polyatomic radicals that can be represented by two coupled two-level systems, large molasseslike cooling forces can be realized using two separated BCF profiles [42]. This suggests that broadband cooling, which combines multiple BCF profiles of the same phase at different detunings, may be feasible in more complicated systems than a single two-level atom. Overall, the most effective method we have found to extend the velocity range of the stimulated forces on two-level atoms is the laser frequency chirp method [35], which can be applied to either bichromatic or polychromatic forces.

## IV. CONCLUSION

We developed a numerical model and Monte Carlo simulations to analyze bichromatic and polychromatic stimulated forces for slowing of Yb atoms under realistic experimental conditions. We have shown theoretically that it is possible to cool and trap Yb atoms on the narrow $^3P_1$ transition and achieve a MOT loading rate in the order of $10^8$ atoms/s using the total laser power of 1 W (Rabi frequency $\Omega$ near 25 MHz).

The square-wave modulation results show great promise. At optimal conditions, this polychromatic force has about the same magnitude but almost twice the velocity range of the bichromatic force. Adding higher harmonics to the square-wave modulation makes the pulses more similar to $\pi$ pulses as shown in the Bloch vector trajectories. This square-wave stimulated force may be realized by modulating either the amplitude or phase of two counterpropagating beams, instead of overlapping four bichromatic cw beams. Splitting total laser power evenly between two beams instead of four partially accounts for the 70% enhancement in the predicted MOT loading rate compared to the chirped BCF method. Our simulation also shows that the square-wave modulation reduces spontaneous emissions by up to 33% compared to the BCF method. This can help prevent heating, especially in atoms with shorter lifetimes, and population loss in multilevel systems and molecules.

Our model has informed optimal experimental design for stimulated slowing and trapping of Yb atoms. Experiments are underway to test and verify these findings. The simulations we developed have flexibility and can be modified to investigate other two-level systems, such as other alkaline-earth-metal-like atoms (e.g., Ca, Sr).

## ACKNOWLEDGMENTS

This research was funded by Office of Naval Research Grant No. N000141712255. Some of the computing was performed on the Sherlock cluster at Stanford University. We would like to thank the Stanford Research Computing Center for providing computational resources and support. T.N. developed the PYTHON codes and simulations used in this work and analyzed the results. T.M.L. and N.R. derived equations for the bichromatic force calculations and developed an earlier computer model of the bichromatic force in MATLAB. L.H. supervised this research. T.N. wrote the manuscript with input from L.H.

[1] N. Poli, C. W. Oates, P. Gill, and G. M. Tino, Optical atomic clocks, La Riv. Nuovo Cimento **36**, 555 (2013).

[2] S. Sugawa, R. Yamazaki, S. Taie, and Y. Takahashi, Bose-Einstein condensate in gases of rare atomic species, Phys. Rev. A **84**, 011610(R) (2011).

[3] H. Hara, Y. Takasu, Y. Yamaoka, J. M. Doyle, and Y. Takahashi, Quantum Degenerate Mixtures of Alkali and Alkaline-Earth-Like Atoms, Phys. Rev. Lett. **106**, 205304 (2011).

[4] J. P. Covey, A. Sipahigil, S. Szoke, N. Sinclair, M. Endres, and O. Painter, Telecom-Band Quantum Optics with Ytterbium Atoms and Silicon Nanophotonics, Phys. Rev. Appl. **11**, 034044 (2019).

[5] J. Rudolph, T. Wilkason, M. Nantel, H. Swan, C. M. Holland, Y. Jiang, B. E. Garber, S. P. Carman, and J. M. Hogan, Large Momentum Transfer Clock Atom Interferometry on the 689 nm Intercombination Line of Strontium, Phys. Rev. Lett. **124**, 083604 (2020).

[6] L. Hu, E. Wang, L. Salvi, J. N. Tinsley, G. M. Tino, and N. Poli, Sr atom interferometry with the optical clock transition as a gravimeter and a gravity gradiometer, Classical Quantum Gravity **37**, 014001 (2019).

[7] T. H. Loftus, Laser cooling and trapping of atomic ytterbium, Ph.D. thesis, University of Oregon, 2001.

[8] T. H. Loftus, A. Vitouchkine, and L. Hollberg, Permanent magnet axial field Zeeman slower, Patent No. US8710428B1, 2014.

[9] E. Wodey, R. Rengelink, C. Meiners, E. Rasel, and D. Schlippert, A robust, high-flux source of laser-cooled ytterbium atoms, J. Phys. B: At., Mol. Opt. Phys. **54**, 035301 (2021).

[10] S. Dörscher, A. Thobe, B. Hundt, A. Kochanke, R. Le Targat, P. Windpassinger, C. Becker, and K. Sengstock, Creation of quantum-degenerate gases of ytterbium in a compact 2D-/3D-magneto-optical trap setup, Rev. Sci. Instrum. **84**, 043109 (2013).

[11] D. Stack, J. Elgin, P. M. Anisimov, and H. Metcalf, Numerical studies of optical forces from adiabatic rapid passage, Phys. Rev. A **84**, 013420 (2011).

[12] J. P. Bartolotta, M. A. Norcia, J. R. K. Cline, J. K. Thompson, and M. J. Holland, Laser cooling by sawtooth-wave adiabatic passage, Phys. Rev. A **98**, 023404 (2018).

[13] M. A. Norcia, J. R. Cline, J. P. Bartolotta, M. J. Holland, and J. K. Thompson, Narrow-line laser cooling by adiabatic transfer, New J. Phys. **20**, 023021 (2018).

[14] N. Petersen, F. Mühlbauer, L. Bougas, A. Sharma, D. Budker, and P. Windpassinger, Sawtooth-wave adiabatic-passage slowing of dysprosium, Phys. Rev. A **99**, 063414 (2019).

[15] J. P. Bartolotta, J. T. Reilly, and M. J. Holland, Speeding up particle slowing using shortcuts to adiabaticity, Phys. Rev. A **102**, 043107 (2020).

[16] J. P. Bartolotta and M. J. Holland, Sawtooth-wave adiabatic passage in a magneto-optical trap, Phys. Rev. A **101**, 053434 (2020).

[17] S. Malinovskaya, Laser cooling using adiabatic rapid passage, Front. Phys. **16**, 52601 (2021).

[18] C.-C. Chen, S. Bennetts, R. González-Escudero, F. Schreck, and B. Pasquiou, Sisyphus optical lattice decelerator, Phys. Rev. A **100**, 023401 (2019).

[19] W. C. Magno, R. L. Cavasso Filho, and F. C. Cruz, Two-photon Doppler cooling of alkaline-earth-metal and ytterbium atoms, Phys. Rev. A **67**, 043407 (2003).

[20] J. Lee, J. H. Lee, J. Noh, and J. Mun, Core-shell magneto-optical trap for alkaline-earth-metal-like atoms, Phys. Rev. A **91**, 053405 (2015).

[21] B. Plotkin-Swing, A. Wirth, D. Gochnauer, T. Rahman, K. E. McAlpine, and S. Gupta, Crossed-beam slowing to enhance narrow-line ytterbium magneto-optic traps, Rev. Sci. Instrum. **91**, 093201 (2020).

[22] E. A. Curtis, C. W. Oates, and L. Hollberg, Quenched narrow-line laser cooling of $^{40}$Ca to near the photon recoil limit, Phys. Rev. A **64**, 031403(R) (2001).

[23] C. Grain, T. Nazarova, C. Degenhardt, F. Vogt, C. Lisdat, E. Tiemann, U. Sterr, and F. Riehle, Feasibility of narrow-line cooling in optical dipole traps, Eur. Phys. J. D **42**, 317 (2007).

[24] O. N. Prudnikov, R. Y. Il'enkov, A. V. Taichenachev, and V. I. Yudin, Scaling law in laser cooling on narrow-line optical transitions, Phys. Rev. A **99**, 023427 (2019).

[25] C.-C. Chen, S. Bennetts, R. G. Escudero, B. Pasquiou, and F. Schreck, Continuous Guided Strontium Beam with High Phase-Space Density, Phys. Rev. Appl. **12**, 044014 (2019).

[26] H. Metcalf, *Colloquium*: Strong optical forces on atoms in multifrequency light, Rev. Mod. Phys. **89**, 041001 (2017).

[27] V. Voitsekhovich, M. Danielko, A. Negriiko, V. Romanenko, and L. Yatsenko, Stimulated light pressure on atoms in counter-propagating amplitude modulated waves, Sov. Phys. JETP **72**, 219 (1991).

[28] R. Grimm, Y. B. Ovchinnikov, A. Sidorov, and V. S. Letokhov, Observation of a Strong Rectified Dipole Force in a Bichromatic Standing Light Wave, Phys. Rev. Lett. **65**, 1415 (1990).

[29] J. Söding, R. Grimm, Y. B. Ovchinnikov, P. Bouyer, and C. Salomon, Short-Distance Atomic Beam Deceleration with a Stimulated Light Force, Phys. Rev. Lett. **78**, 1420 (1997).

[30] M. R. Williams, F. Chi, M. T. Cashen, and H. Metcalf, Measurement of the bichromatic optical force on Rb atoms, Phys. Rev. A **60**, R1763 (1999).

[31] M. R. Williams, F. Chi, M. T. Cashen, and H. Metcalf, Bichromatic force measurements using atomic beam deflections, Phys. Rev. A **61**, 023408 (2000).

[32] T. C. Liebisch, E. Blanshan, E. A. Donley, and J. Kitching, Atom-number amplification in a magneto-optical trap via stimulated light forces, Phys. Rev. A **85**, 013407 (2012).

[33] M. Cashen, O. Rivoire, V. Romanenko, L. Yatsenko, and H. Metcalf, Strong optical forces in frequency-modulated light, Phys. Rev. A **64**, 063411 (2001).

[34] M. Partlow, X. Miao, J. Bochmann, M. Cashen, and H. Metcalf, Bichromatic Slowing and Collimation to Make an Intense Helium Beam, Phys. Rev. Lett. **93**, 213004 (2004).

[35] M. A. Chieda and E. E. Eyler, Bichromatic slowing of metastable helium, Phys. Rev. A **86**, 053415 (2012).

[36] M. A. Chieda and E. E. Eyler, Prospects for rapid deceleration of small molecules by optical bichromatic forces, Phys. Rev. A **84**, 063401 (2011).

[37] S. E. Galica, L. Aldridge, and E. E. Eyler, Four-color stimulated optical forces for atomic and molecular slowing, Phys. Rev. A **88**, 043418 (2013).

[38] D. Dai, Y. Xia, Y. Fang, L. Xu, Y. Yin, X. Li, X. Yang, and J. Yin, Efficient stimulated slowing and cooling of the magnesium fluoride molecular beam, J. Phys. B: At., Mol. Opt. Phys. **48**, 085302 (2015).

[39] E. Ilinova, J. Weinstein, and A. Derevianko, Stimulated deceleration of diatomic molecules on multiple rovibrational transitions with coherent pulse trains, New J. Phys. **17**, 055003 (2015).

[40] L. Aldridge, S. E. Galica, and E. E. Eyler, Simulations of the bichromatic force in multilevel systems, Phys. Rev. A **93**, 013419 (2016).

[41] Y. Yin, S. Xu, M. Xia, Y. Xia, and J. Yin, Optically stimulated slowing of polar heavy-atom molecules with a constant beat phase, Phys. Rev. A **97**, 043403 (2018).

[42] K. Wenz, I. Kozyryev, R. L. McNally, L. Aldridge, and T. Zelevinsky, Large molasses-like cooling forces for molecules using polychromatic optical fields: A theoretical description, Phys. Rev. Research **2**, 043377 (2020).

[43] I. Kozyryev, L. Baum, L. Aldridge, P. Yu, E. E. Eyler, and J. M. Doyle, Coherent Bichromatic Force Deflection of Molecules, Phys. Rev. Lett. **120**, 063205 (2018).

[44] S. E. Galica, L. Aldridge, D. McCarron, E. E. Eyler, and P. L. Gould, Deflection of a molecular beam using the bichromatic stimulated force, Phys. Rev. A **98**, 023408 (2018).

[45] A. Goepfert, I. Bloch, D. Haubrich, F. Lison, R. Schütze, R. Wynands, and D. Meschede, Stimulated focusing and deflection of an atomic beam using picosecond laser pulses, Phys. Rev. A **56**, R3354 (1997).

[46] E. Ilinova, M. Ahmad, and A. Derevianko, Doppler cooling with coherent trains of laser pulses and a tunable velocity comb, Phys. Rev. A **84**, 033421 (2011).

[47] X. Long, S. S. Yu, A. M. Jayich, and W. C. Campbell, Suppressed Spontaneous Emission for Coherent Momentum Transfer, Phys. Rev. Lett. **123**, 033603 (2019).

[48] L. Yatsenko and H. Metcalf, Dressed-atom description of the bichromatic force, Phys. Rev. A **70**, 063402 (2004).

[49] A. Guttridge, S. A. Hopkins, S. L. Kemp, D. Boddy, R. Freytag, M. P. A. Jones, M. R. Tarbutt, E. A. Hinds, and S. L. Cornish, Direct loading of a large Yb MOT on the $^1S_0 \rightarrow {}^3P_1$ transition, J. Phys. B: At., Mol. Opt. Phys. **49**, 145006 (2016).

[50] J. R. Johansson, P. D. Nation, and F. Nori, QuTiP: An open-source Python framework for the dynamics of open quantum systems, Comput. Phys. Commun. **183**, 1760 (2012).

[51] J. R. Johansson, P. D. Nation, and F. Nori, QuTiP 2: A Python framework for the dynamics of open quantum systems, Comput. Phys. Commun. **184**, 1234 (2013).

[52] V. Minogin and O. Serimaa, Resonant light pressure forces in a strong standing laser wave, Opt. Commun. **30**, 373 (1979).

[53] A. Kawasaki, B. Braverman, Q. Yu, and V. Vuletic, Two-color magneto-optical trap with small magnetic field for ytterbium, J. Phys. B: At., Mol. Opt. Phys. **48**, 155302 (2015).

[54] J. Hoffnagle, Proposal for continuous white-light cooling of an atomic beam, Opt. Lett. **13**, 102 (1988).

[55] H. Wallis and W. Ertmer, Broadband laser cooling on narrow transitions, J. Opt. Soc. Am. B **6**, 2211 (1989).

[56] M. Zhu, C. W. Oates, and J. L. Hall, Continuous High-Flux Monovelocity Atomic Beam Based on a Broadband Laser-Cooling Technique, Phys. Rev. Lett. **67**, 46 (1991).

[57] M. Watanabe, R. Ohmukai, U. Tanaka, K. Hayasaka, H. Imajo, and S. Urabe, Velocity control of an Yb beam by a frequency-doubled mode-locked laser, J. Opt. Soc. Am. B **13**, 2377 (1996).

[58] T. H. Loftus, T. Ido, M. M. Boyd, A. D. Ludlow, and J. Ye, Narrow line cooling and momentum-space crystals, Phys. Rev. A **70**, 063413 (2004).